
Article:
Martin-Short, R., Hill, Jon orcid.org/0000-0003-1340-4373, Kramer, S.C. et al. (2 more authors) (2015) Tidal resource extraction in the Pentland Firth, UK:Potential impacts on flow regime and sediment transport in the Inner Sound of Stroma. Renewable Energy. 596–607. ISSN 0960-1481

https://doi.org/10.1016/j.renene.2014.11.079

Renewable Energy 76 (2015) 596–607

Contents lists available at ScienceDirect

Renewable Energy

journal homepage: www.elsevier.com/locate/renene

Tidal resource extraction in the Pentland Firth, UK: Potential impacts on flow regime and sediment transport in the Inner Sound of Stroma

R. Martin-Short [a], J. Hill [a, *], S.C. Kramer [a], A. Avdis [a], P.A. Allison [a], M.D. Piggott [a, b]

[a] Applied Modelling and Computation Group, Department of Earth Science and Engineering, Imperial College London, SW7 2AZ, UK
[b] Grantham Institute for Climate Change, Imperial College London, SW7 2AZ, UK

ARTICLE INFO

Article history:
Received 29 August 2013
Accepted 22 November 2014
Available online

Keywords:
Tidal energy
Modelling
Pentland Firth
Finite element

ABSTRACT

Large-scale extraction of power from tidal streams within the Pentland Firth is expected to be underway in the near future. The Inner Sound of Stroma in particular has attracted significant commercial interest. To understand potential environmental impacts of the installation of a tidal turbine array a case study based upon the Inner Sound is considered. A numerical computational fluid dynamics model, Fluidity, is used to conduct a series of depth-averaged simulations to investigate velocity and bed shear stress changes due to the presence of idealised tidal turbine arrays. The number of turbines is increased from zero to 400. It is found that arrays in excess of 85 turbines have the potential to affect bed shear stress distributions in such a way that the most favourable sites for sediment accumulation migrate from the edges of the Inner Sound towards its centre. Deposits of fine gravel and coarse sand are indicated to occur within arrays of greater than 240 turbines with removal of existing deposits in the shallower channel margins also possible. The effects of the turbine array may be seen several kilometres from the site which has implications not only on sediment accumulation, but also on the benthic fauna.

1. Introduction

Electricity generation from turbines driven by tidal currents present an attractive form of renewable energy, which is highly reliable and abundant in many coastal regions [8,13]. The UK is known to boast a significant proportion of Europe's extractable tidal resource, a large part of which is found in the Pentland Firth [8,45]. The Pentland Firth, shown in Fig. 1, lies at the northern tip of Scotland separating the Orkney Islands from the mainland to the south. This region is well known for the high speed of its tidal currents [14], and has consequently attracted significant attention as a possible site for the placement of tidal stream generators [45]. Promising regions for development are the Inner Sound, Outer Sound and South Ronaldsay Channel, shown in Figs. 1 and 2. Tidal currents within this region are influenced by local bathymetry and coastline, which ultimately determines their speed and direction [45].

The tidal regime in this area is dominated by the M2 component and thus involves a semi-diurnal exchange of water between the North Sea and Atlantic Ocean [45]. Tidal current velocities are at their greatest within the Outer Sound, with a mean spring velocity of just under 3 ms^{-1} and current speeds exceeding 1 ms^{-1} for 80% of each tidal cycle [45]. The Inner Sound and South Ronaldsay Channel also exhibit a useful tidal resource [8,13]. Commercial exploitation of this resource is expected to begin shortly with the planned placement of a demonstration array of 1 MW rated tidal turbines in the Inner Sound by MeyGen Ltd., based upon plans published in 2011 [44]. This would mark the beginning of a staged development process, which may ultimately see the operation of a 398 MW turbine array within the Inner Sound in the coming decades [44].

Previous studies of tides in the Pentland Firth suggest that it features significant tidal asymmetry, with maximum current velocities during flood tide being up to 2 ms^{-1} higher than those during ebb tide [18,45]. The nature of this asymmetry within the Inner Sound is discussed in Ref. [17] which presents the results of two Acoustic Doppler Current Profiler (ADCP) surveys of the Inner Sound. During flood tide, currents tend to flow west-east, and are concentrated within a distinct 'core' about 1 km south of Stroma [17]. During ebb tide currents flow east-west, the 'core' appears to

* Corresponding author. Environment Department, University of York, Heslington, York, YO10 5DD, UK. Tel.: +44 (0) 1904 324480; fax: +44 (0) 1904 322998.
E-mail address: jon.hill@york.ac.uk (J. Hill).

http://dx.doi.org/10.1016/j.renene.2014.11.079

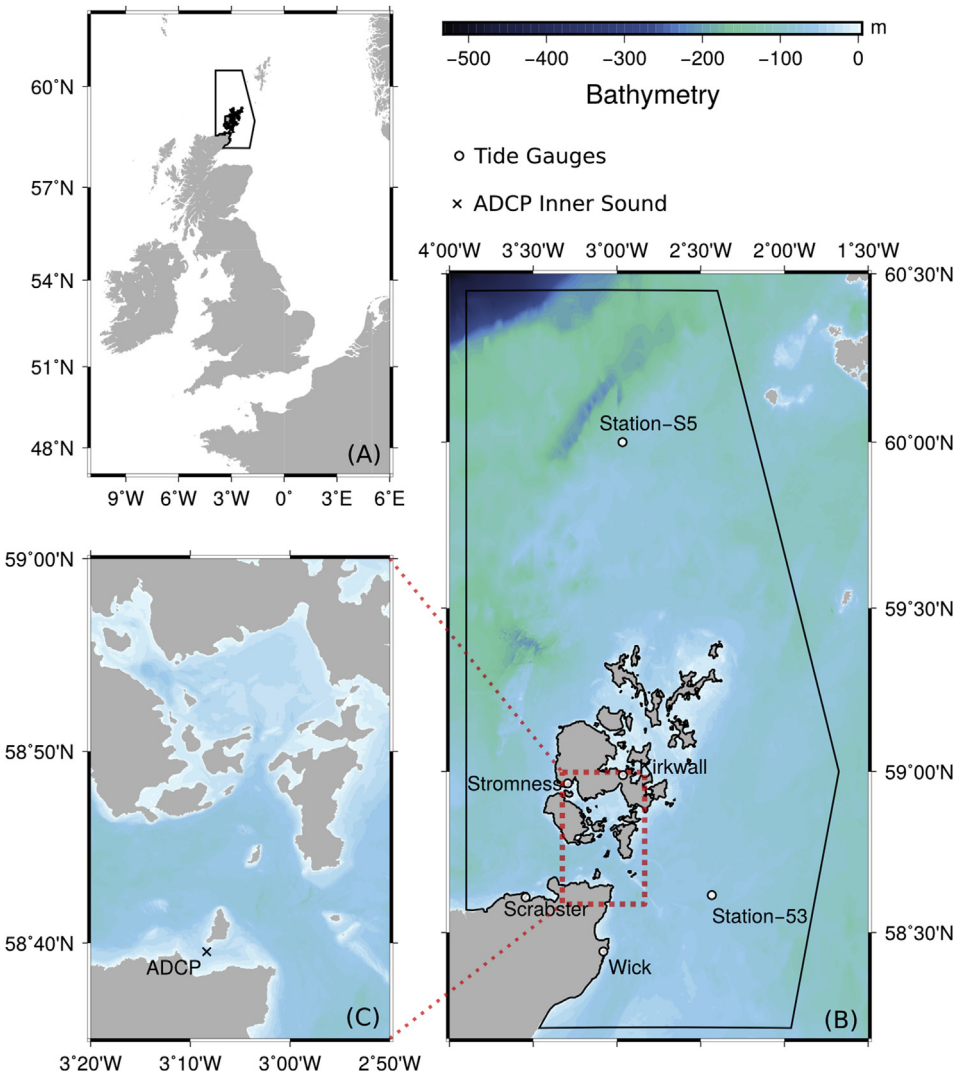

Fig. 1. Maps showing study location and simulated domain. A) Map of North-West Europe centred around the North Sea. B) Map of the simulation domain, the circular markers show the locations of tidal gauges. The thick outline (A and B) delineates the simulation domain and colour relief represents the resampled bathymetry used in this study. C) Map of the Pentland Firth and surrounding islands, the × marker show the location of the Acoustic Doppler Current Profiler (ADCP). (For interpretation of the references to colour in this figure legend, the reader is referred to the web version of this article.)

be less distinct, and is located significantly further north. [17] also report the results of a sidescan sonar survey of the sea bed, which clearly indicates the presence of sedimentary structures concentrated in regions of low current velocities. Such results contrast with geological maps of the region, which suggest that the Pentland Firth is entirely composed of exposed bedrock [45]. Although the overall regime here is clearly erosional, very little is known about local scale variations in sediment transport, which serves to reinforce the need to understand these phenomena before the construction of tidal arrays gets underway. In order to begin to address such issues [17] construct a sediment transport model of the Inner Sound using the MIKE21 software package [47]. However Ref. [17], did not include the effects of tidal energy arrays in their study, but did show locations of sediment accumulation.

Many studies have indicated that the presence of a tidal turbine array within such a channel can have a significant influence on the flow regime and thus must be taken into account when attempting to assess the total extractable resource [2,37,38,46]. Of particular interest to this study is the potential ability of a turbine array to divert peak flows away from their natural path and thus alter patterns of erosion and deposition of sediment within the channel. Previous work, such as the 1D simulation carried out by Ref. [38] suggest that changes to the sediment transport regime may be particularly significant if the tidal currents are asymmetric, at least in estuarine environments. In such a tidal regime the net movement of sediment can occur in either the ebb or flood direction [38]. The effects of tidal energy converters on sediment transport may be seen several kilometres from the site of the energy converters. Effects are commonly categorised as near-field (<1 km), far-field (1–10 km) and regional (>10 km) [46]. Modelling studies on a sand-dominated system around Alderney, just off the coast of France, showed the potential effects on sediment movement could cover over 100 km^2 [37]. The effect is not limited to open marine systems, such as around Alderney, with estuarine environments also similarly affected [2]. Moreover Ref. [2], showed that the presence of turbines could also affect the distribution of faecal bacteria in the Severn Estuary, which is closely associated with sediment.

Movement of sediment into and out of areas can affect the local fauna [46] and is therefore an important component of any site

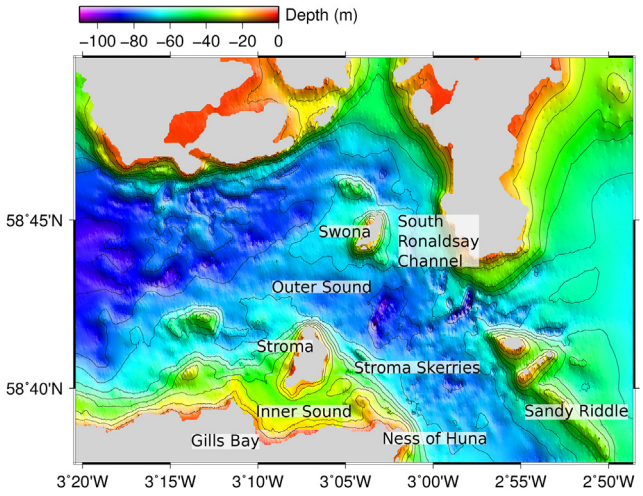

Fig. 2. Bathymetric map of the Pentland Firth, showing the locations of three potentially important channels for tidal resource extraction. ©Crown Copyright/SeaZone Solutions. All Rights Reserved. Licence No. 052006.001 31st July 2011. Not to be used for Navigation.

assessment. According to past surveys of the Orkney Isles, the sea bed in the area is dominated by rocky sea bed [9,30,45] which is classified as "Atlantic and Mediterranean high energy infralittoral rock" under the EUNSIS 2007-11 scheme, whilst sediment in the area is poorly to moderately well sorted, dominated by coarse sands and fine gravels [4]. In addition, there are gravel-sized benthic bioclasts on the North-East Orkney shelf, dominated by bivalves, barnacles, bryozoa and calcareous worms [21] and similar bioclasts are to be expected in the Pentland Firth as well. There will also be a supply of suspended sediment, though this is poorly understood, but values of 0.1–39 mg/l are thought to be derived from the North Sea [30] and similar values may flush through the Pentland Firth. Recent surveys have shown clear sediment banks in and around the Isle of Stroma (Fig. 3 and [17]), where this study has focused. Sidescan sonar data collected in the area show several distinctive sedimentary features ranging from small-scale ripples to large waveforms [17]. Data collected by MeyGen Ltd. (Fig. 3) indicates the presence of a relatively large, elongated region of sediment extending east from the southern tip of Stroma and is roughly consistent with [17]. Given the presence of dunes and the close proximity to known coarse sediment accumulations such as Sandy Riddle to the south-east [4], it is reasonable to assume that this feature is composed mainly of coarse sand and fine gravel. Such sediment is likely to be rich in carbonate material such as shell fragments, the potential sources of which are described by Ref. [21].

Numerical modelling is currently the only viable way of assessing the possible impact of tidal marine energy converters before their placement. A number of studies have attempted to do this in various locations using a wide variety of models. However, few have been able to place individual turbines within the flow due

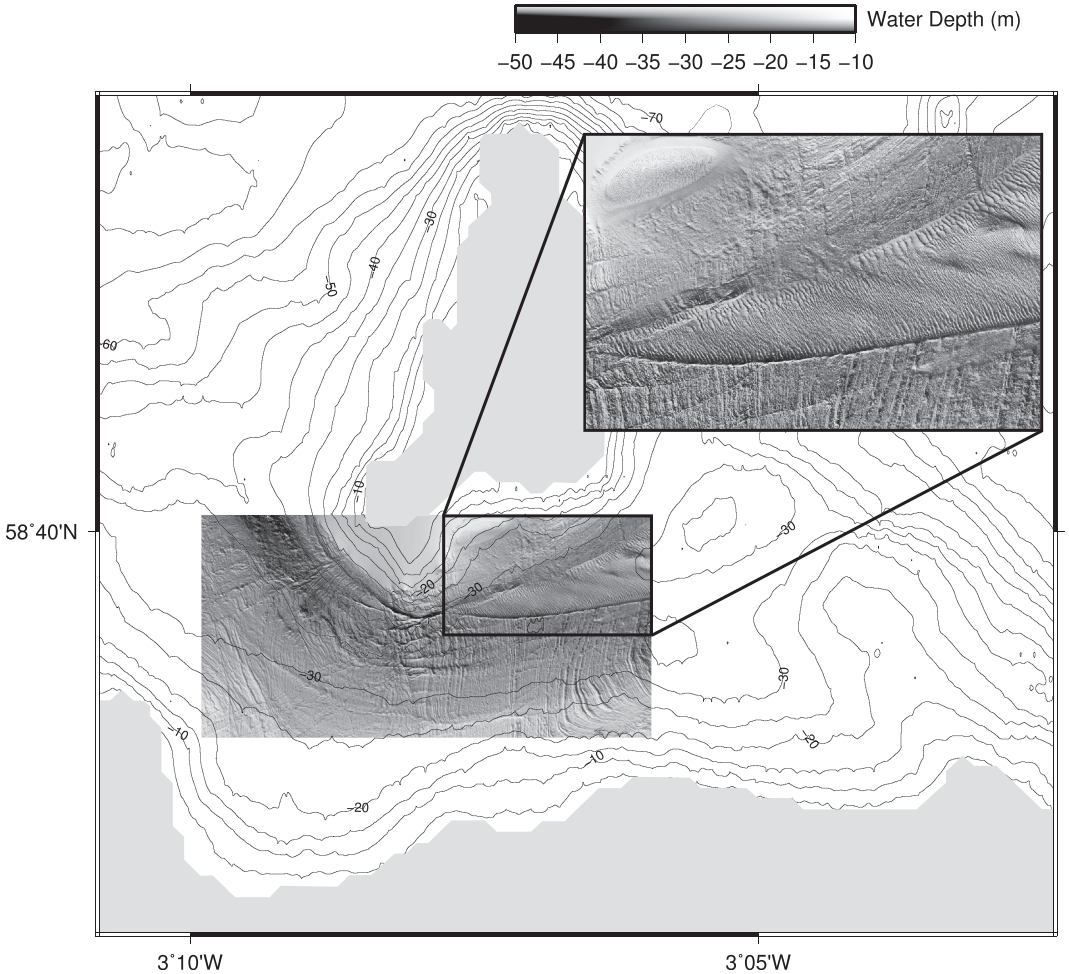

Fig. 3. High resolution bathymetry of the Inner Sound. This image reveals the presence of a bar of coarse sediment east of Stroma. Sediment is also likely to accumulate in Gills Bay (lower left) and within the embayment at the southern tip of Stroma Bathymetry obtained from MeyGen Ltd.

to constraints on spatial mesh resolution. The ability to model all scales, from the regional scale (10–100 km) down to the near-field scale (1–10 km) and further into the fine scale regions around turbines (m scale), requires a computational model that can handle multiscale resolution. Previous efforts at tidal modelling have used nested models [27,32] or simply not been capable of modelling a large area with sufficient resolution in the region of interest. [27] use a finest resolution of 1.5 km, whereas [32] use a resolution of 200 m for their idealised case. There are also numerical difficulties with using a nested model with tides [32]. Therefore, a common approach for multiscale modelling is to use unstructured meshes with either finite volume or finite element discretisation methods. A few assessments of potential sites for tidal turbines have been previously made with such models (e.g. Refs. [5,17,18]), however they are still generally limited in the size of regional domain or have relatively coarse resolution near to the array.

This paper describes a numerical modelling study carried out using Fluidity [22,39,40,43], a model that offers both depth-averaged and three-dimensional, non-hydrostatic approximations. It employs finite-element discretisations on unstructured meshes and hence is capable of using resolutions that can vary from sub-metre to 10's of kilometres within the same simulation. We first briefly describe the governing equations underlying the shallow water model used in this work, their discretisation within Fluidity, and describe the simulation setup, including mesh generation. A validation of the Fluidity model as applied to this problem is then presented. Several separate simulations were carried out, each with different numbers of tidal energy converters within the study site. In contrast to previous tidal turbine studies, Fluidity is capable of resolving individual turbines as a finite area embedded in the mesh. From these simulations we describe the potential impacts that the placement of tidal energy converters in this region may have on sediment transport and on the flow regime, a result lacking from previous studies.

2. Numerical model and problem setup

2.1. Fluidity

Fluidity is a highly flexible finite element/control volume modelling framework which allows for the numerical solution of a number of equation sets [42] and has been used in a variety of flow studies ranging from laboratory-to ocean-scale (e.g. Refs. [28,29,50]. In an ocean modelling context, Fluidity has been used to model both modern and ancient tides on regional and global scales [34,48–50]. Here, the depth-averaged shallow water equations are solved in a rotating reference frame in non-conservative form:

$$\frac{\partial \boldsymbol{u}}{\partial t} + \boldsymbol{u}\cdot\nabla\boldsymbol{u} + f\boldsymbol{u}^T - \nabla\nu\left[\nabla\boldsymbol{u} + (\nabla\boldsymbol{u})^T\right] + g\nabla\eta = -(c_b + c_t)\frac{||\boldsymbol{u}||\boldsymbol{u}}{H}, \frac{\partial\eta}{\partial t} + \nabla\cdot(H\boldsymbol{u}) = 0, \quad (1)$$

where $\boldsymbol{u}$ is the 2D, depth-averaged velocity vector, t represents time, η is the free surface perturbation, H is the total water depth, and ν is the kinematic viscosity. The Coriolis term, $f\boldsymbol{u}^T$, consists of $\boldsymbol{u}^T$, the velocity vector rotated counter-clockwise over 90°, and $f = 2\Omega\sin(\zeta)$, with Ω the angular frequency of Earth's rotation and ζ the latitude. The dimensionless friction coefficients c_b and c_t represent respectively the background bottom drag (assumed constant here) and an enhanced drag field used to parameterise the effect of the individual turbines (see Section 2.4).

The equation (1) is discretised using a mixed finite element pair, with a piecewise linear discontinuous Galerkin approximation ($P1_{DG}$) for velocity and a continuous Galerkin, piecewise quadratic formulation for the free surface (P2). The resulting $P1_{DG}P2$ velocity/free-surface discretisation has a number of desirable properties described fully in Refs. [10–12]. In addition to the discretisation of the linear shallow water terms described therein, we employ a standard $P1_{DG}$-discretisation with upwind fluxes and slope limiting [33] for the advection term and the Compact Discontinuous Galerkin scheme (CDG, see Refs. [41]), for the viscosity term.

A two-level θ method is employed for time-integration, combined with explicit subcycling for the advection step. Here $\theta = 0.53$, which is close to the Crank-Nicolson scheme, and therefore minimises wave dissipation whilst maintaining stability. Two Picard iterations per time-step are used to linearise the nonlinearity in the advection and friction terms. Finally, the linear discretised systems are solved using iterative sparse linear solvers available in PETSc [3]. More details on the spatial and temporal discretisations available in Fluidity are described in Imperial College London, [31] and [42].

2.2. Mesh generation

The simulation domain, shown in Fig. 1, is bounded by the parallels at 58°:12′*N* and 60°:27′*N*. The Eastern side of the domain is at the meridian through 3°:54′*E* and the western side of the domain is composed of constant bearing lines through points (2°:24′*E*,60°:27′*N*) to (1°:40′:30″*E*,59°*N*) and (1°:40′:30″*E*,59°*N*) to (1°:57′:36″*E*,58°:12′*N*). The open boundaries were chosen to be far enough from the area of interest, the Inner Sound of the Pentland Firth, to minimise boundary effects. Moving the boundaries even

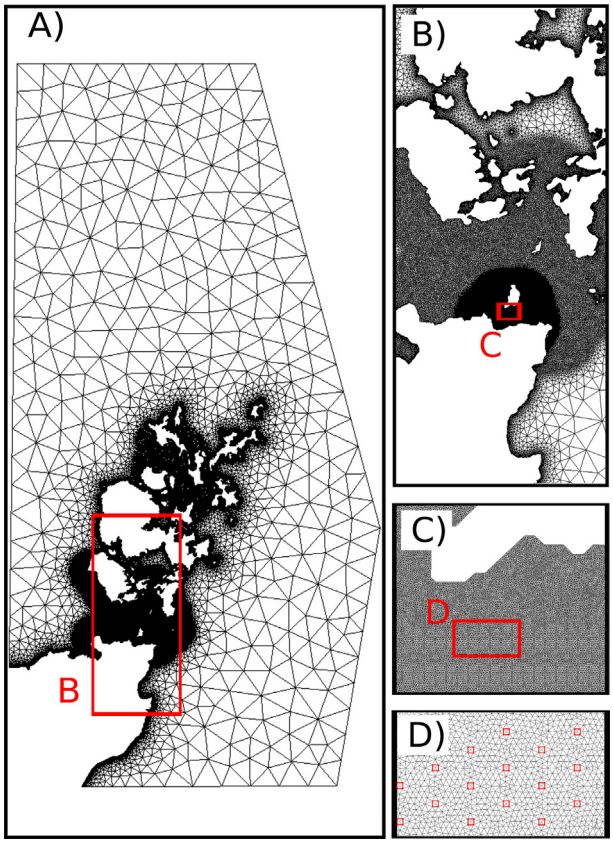

Fig. 4. The mesh used in this study, containing 379,368 nodes and 758,904 elements. A) Overall view. B) View of the Pentland Firth, and Scapa flow between the islands of Hoy and South Ronaldsay. C) View of the 18 m–resolution, Inner Sound region south of Stroma island. D) Zoom of an area of the turbine array with individual turbines highlighted.

further away was shown not to have a significant impact on the validation results. The coastlines were extracted from the "full resolution" data from the GSHHS database [51]. The bathymetry data was obtained from the Ref. [19], at a one arcsec resolution ($\approx$30 m).

Unstructured meshes are able to accurately represent complicated coastline shapes and thus offer significant advantages over traditional structured meshes in ocean modelling [49]. The mesh used in this study, shown in Fig. 4, was generated by Gmsh [25]. The mesh is generated in the UTM30V coordinate reference system and contains 379,368 nodes and 758,904 triangular elements. Mesh resolution varies from 20 km far from the coastline to 18 m at the turbine array. Fig. 4 (B) and (C) shows the mesh gradation to successively higher resolution: The elements in the Pentland Firth between Hoy island, South Ronaldsay and mainland Scotland have an edge length of 250 m and elements around the Inner Sound have an edge length of 18 m. Elements at coastlines of other areas have an edge length of 100 m.

The minimum edge length of 18 m in the Inner Sound, allows the incorporation of square areas in the mesh to represent each turbine individually, of exactly the turbine diameter ($D_t = 18$ m). Each square is then split into four equilateral triangles in the mesh (Fig. 4D). The number of these mesh squares corresponds to the maximum number of turbine that were employed in this study. As explained in Section 2.4, the turbines were parameterised using an increased bottom friction in the squares. In runs with smaller numbers of turbines the same mesh with the same set of squares was used but the bottom friction was not increased in all of them.

2.3. Sediment erosion and deposition

Given the uncertainties in the suspended and bedload sediment supply in and out of the region, coupled with a lack of data on current sediment deposits, it is difficult to model suspended and bedload transport due to lack of boundary conditions. It is possible however, to gain significant insight into the sediment transport regime of a region by looking at the distribution of bed shear stress as this is the major control on sediment movement [34,53]. This approach has been used previously to look at the distribution of sediments in the ancient past using Fluidity [34]. The bed shear stress can be used to determine the *finest* grain size that can be deposited in a region and is a critical first step to modelling suspended and bedload sediment transport. Given the short duration of the modelling study here, the changes to bed height are negligible over this period and hence will have a negligible effect on the flow and are thus not considered. Bed shear stress is calculated using:

$$\boldsymbol{\tau} = \rho C_d ||\boldsymbol{u}|| \boldsymbol{u}, \tag{2}$$

where $||\boldsymbol{u}||$ is the magnitude of velocity vector $\boldsymbol{u}$, ρ is the density of seawater (assumed to be 1025 kgm^{-1}) and C_d is the bottom drag coefficient [34]. A constant value of 0.0025 was chosen to match the values given in Ref. [6]. This drag coefficient is only used in calculating bed shear stress and a different value is used for calibrating the flow velocity (see Section 2.5). Given the value of critical shear stress (τ_c) for the sediment of interest, one can use the distribution of bed shear stress to determine the likely locations of erosion and deposition of that sediment type. The critical shear stress is related to the grain diameter (D) via the critical Shields parameter (β_c). This is given by

$$\beta_c = \frac{\tau_c}{g\left(\rho_{\text{grain}} - \rho_{\text{fluid}}\right)D}. \tag{3}$$

Table 1
Mean critical shear stress (τ_c) conditions for the entrainment of various sediment grain sizes (D) from Ref. [6]. Given the high current velocities within the Pentland Firth, one might expect gravel to be the dominant sediment type here.

Class name	Diameter (mm)	Critical shear stress (Pa)	Critical velocity (ms^{-1})
Coarse gravel	16–32	12.2–26.0	2.16–3.19
Medium gravel	8.0–16	5.7–12.2	1.49–2.16
Fine gravel	2.0–8.0	1.26–5.70	0.701–1.49
Coarse sand	0.5–2.0	0.27–1.26	0.325–0.701
Medium sand	0.25–0.5	0.194–0.27	0.275–0.375

Although an exact value for β_c is often difficult to determine, we use the values report in Ref. [6]. Table 1 displays values of τ_c for various grades of sediment. The value of ρ_{grain} is taken to be 2650 kgm^{-3}, which is the density of quartz, and ρ_{fluid} is 1025 kgm^{-3}. Note that the sediment in the region is likely to be non-spherical and have densities that vary depending on the organism from which the bioclast was formed. However, these uncertainties in values are not expected to have a significant effect on the results presented here.

2.4. Turbine parameterisation

Within the mesh the tidal turbines are represented as square regions of 18 m in width, which is the same as the diameter of the horizontal axis turbines described in Ref. [44]. These square regions are imposed as constraints in the mesh generation procedure, with edges of triangles exactly matching these rectangular regions. The simplest method of parameterisation involves modelling the turbines as individual regions of increased bottom drag; an approach that is frequently adopted in large-scale tidal array modelling [38] with depth-averaged models.

The drag force applied to the flow by the turbine is typically characterised as a quadratic drag law given by:

$$\boldsymbol{F}(\boldsymbol{u}) = \frac{1}{2}\rho A_t C_t(||\boldsymbol{u}||)||\boldsymbol{u}||\boldsymbol{u}, \tag{4}$$

where C_t is the thrust coefficient of the turbine, a function of the current speed, and A_t its cross-sectional area. The thrust coefficient is not necessarily constant due to, for instance, cut-in velocities and power rating. Here, we have implemented an idealised thrust curve with a cut-in velocity, u_{in}, of 1.0 ms^{-1}, and a constant thrust coefficient with a value of 0.6 between the cut-in velocity and the rated velocity, u_{rated}. Above the rated velocity, the thrust coefficient decreases to maintain a constant power yield in that region. Using actuator disc theory [24], the power can be computed as (neglecting any blockage effects):

$$P(u) = \frac{1}{2}\rho C_P(u) A_t u^3, \quad \text{where} \quad C_P(u) = \frac{1}{2}\left(1 + \sqrt{1 - C_t(u)}\right)C_t(u). \tag{5}$$

The thrust curve that maintains a power output of $P(u) = P(u_{\text{rated}})$ exactly for $u > u_{\text{rated}}$, involves the inversion of a higher order polynomial equation. Here, we have simplified the curve to an inverse cube of the speed, neglecting the variations in Ref. $C_P(u)$ given in (5). As can be seen in Fig. 5, the differences between the simplified curve and curve with exact constant power are small; we feel that this an acceptable approximation for use here given that we are considering an idealised turbine, it could easily be improved using a thrust curve from a real device which would not exactly match the above theory either. The simplified curve we use here is thus given by:

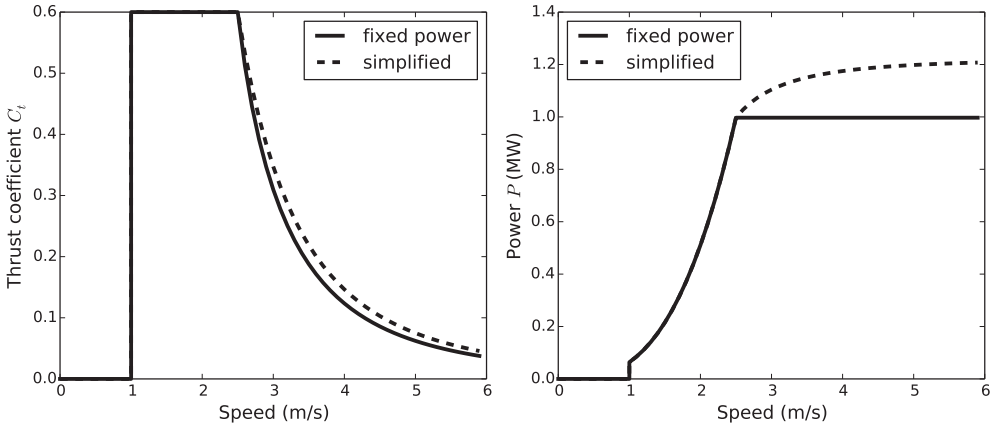

Fig. 5. Thrust (left) and power curve (right) for tidal turbines with a cut-in speed of $u_{\text{in}} = 1.0$ m/s, and a rated speed of $u_{\text{rated}} = 2.5$ m/s. The solid line indicates the thrust curve that leads to a power yield that is exactly constant above the rated speed: $u > u_{\text{rated}}$. The dashed line indicates the simplified formula, equation (6), used in this study.

$$C_t(u) = \begin{cases} 0 & \text{if } u \le u_{\text{in}} \\ \overline{C}_t & \text{if } u_{\text{in}} \le u \le u_{\text{rated}} \\ \overline{C}_t \dfrac{u_{\text{rated}}^3}{u^3} & \text{if } u \ge u_{\text{rated}} \end{cases}, \tag{6}$$

where we use $\overline{C}_t = 0.6, u_{\text{in}} = 1.0$ m/s, and $u_{\text{rated}} = 2.5$ m/s. With turbine cross section $A_{\text{t}} = \pi(D_{\text{t}}/2)^2$ and diameter $D_{\text{t}} = 18$ m, this gives a rated power of $P(u_{\text{rated}}) \approx 1$ MW.

In addition, we have taken into account the drag of the support structure. Although various designs are being considered by turbine manufacturers, for simplicity we have implemented the drag equivalent to a pylon with a drag coefficient of $C_{\text{support}} = 0.7$, which is a typical value for flow past a cylinder at high Reynolds numbers, and a cross section of $A_{\text{support}} = 3.5\times(H + h)$, where $(H + h)$ is the total water depth and we assume a pylon diameter of 3.5 m. Thus the total drag force is given by

$$\boldsymbol{F}(\boldsymbol{u}) = \frac{1}{2}\rho\left(A_t C_t(||\boldsymbol{u}||) + A_{\text{support}} C_{\text{support}}\right)||\boldsymbol{u}||\boldsymbol{u}. \tag{7}$$

The enhanced bottom drag, $c_{\text{t}} > 0$ in (1), applied over a square with area $A_{\text{square}} = D_t^2$ acts like a momentum sink:

$$\int_{\text{square}} \rho c_t ||\boldsymbol{u}||\boldsymbol{u}. \tag{8}$$

We choose the bottom friction coefficient c_{t} such that this sink term is equal to the force in (7), averaged over the square:

$$c_t = \frac{A_t C_t(||\boldsymbol{u}||) + A_{\text{support}} C_{\text{support}}}{2A_{\text{square}}}. \tag{9}$$

The turbines were placed in an array of 10 rows (in the east-west direction) of 40 turbines with a distance of six diameters in each direction. To create a staggered layout, the turbines in the even-numbered columns where then shifted three diameters to the North, thus effectively creating 10 rows of 20 turbines in the odd numbered columns, and staggered in between them 10 rows of 20 turbines from the even numbered columns. The distance, in the east-west direction, between the turbines in each of the 20 staggered rows thereby becomes 12 diameters.

Such a staggered approach, with devices placed at a suitable distance such that their mutual influence is minimised, has been shown to lead to an increased power output [15]. The distances between the rows were chosen here such that 400 turbines could fit in the zone of highest current velocities. Additionally, the rather large distance in east-west direction was chosen to minimise the effect of turbines placed in the wake of upstream turbines, since the accuracy of the modelling of wakes is necessarily limited in a large-scale depth-averaged model. However, we note that finding the true optimal layout of the turbine is a very complex problem [23] that needs to take into account the actual local current direction (which is not exactly east-west in this case) and how that changes after the placement of the turbines. Furthermore, there will be various restrictions on where turbines can be placed due to licensing and bathymetry constraints. For further discussions on the important topic of array staggering and spacing see Ref. [35].

It should be noted that the full layout of 400 turbines used in this idealised scenario extends further east than the existing lease area for the Inner Sound. For runs in this work where the number of turbines, N, is smaller than 400, the identical mesh incorporating 400 square regions is employed but now the bottom friction is only increased in the N western most squares.

2.5. Simulation setups

A suite of simulations featuring arrays of 85, 240 and 400 turbines was setup for this study. The results of these were then compared with one another and with those from a simulation in which no turbines are present, giving four simulations in total. Each simulation features eight tidal components (M2, S2, K1, O1, N2, K2, P1 and Q1). Using the OSU Tidal Software (OTPS, [20]), the free surface elevation was reconstructed and applied as a free surface boundary condition along the open boundaries (Fig. 4).

In order to assess potential regions of sediment accumulation and erosion, Fluidity was set up to output both the instantaneous, mean and maximum bed shear stress at each node in the domain. Of these, the maximum bed shear stress distribution is perhaps the most influential in determining long term patterns of erosion and sedimentation [34].

2.6. Calibration and model validation

A comparison was made between the predicted tides and measured data at a number of gauge locations (see Fig. 1). In addition the currents measured at a fixed ADCP location in the area of interest were compared with the model output.

At the gauge locations amplitude and phases of the main harmonic constituents were available. These were compared with those obtained from a harmonic analysis of 30 days of model output

Table 2
Comparison of main harmonic constituents obtained from a harmonic analysis of model output, run with bottom friction $c_b = 0.005$, compared with harmonic constituents available at 6 different gauges [36]. For each constituent the left column displays the amplitude in meters, and the right column the phase in degrees.

		M2		S2		N2		K1		O1	
Scrabster	Gauge	1.35	243	0.49	276	0.27	219	0.14	137	0.11	347
	Model	1.31	241	0.60	273	0.26	216	0.08	141	0.09	356
Stromness	Gauge	0.90	271	0.35	304	0.18	247	0.11	156	0.10	6
	Model	0.84	268	0.39	300	0.17	246	0.07	155	0.09	12
Kirkwall	Gauge	0.81	295	0.32	341	0.16	276	0.11	158	0.10	19
	Model	0.84	295	0.37	329	0.17	271	0.07	168	0.09	25
Wick	Gauge	1.02	322	0.35	0	0.20	302	0.11	176	0.11	28
	Model	1.01	321	0.45	356	0.21	296	0.07	174	0.10	28
Station-S5	Gauge	0.69	253	0.26	285	0.14	232	0.10	147	0.08	15
	Model	0.71	252	0.33	284	0.15	229	0.06	151	0.07	18
Station-53	Gauge	0.76	326	0.27	4	0.16	304	0.08	186	0.10	32
	Model	0.86	325	0.39	0	0.18	301	0.06	177	0.09	33

at the same locations. The result of this comparison can be seen in Table 2. The amplitudes are fairly well matched in most locations. The largest error seems to appear at *Station-53*, which is furthest from the area of interest, where the model significantly over predicts the tidal signal.

The tidal currents in the Pentland Firth are for a large part driven by a phase difference in the tides across the channel. This can be seen in the table comparing the phases of Scrabster and Stromness with those at Wick and Station-53. The fact that these phases are closely matched by the model gives confidence in the representation of main driving mechanism of the flow in the Pentland Firth.

Some other authors [18,1,5]; have commented on the influence of the choice of bottom friction coefficient on the representation of currents in depth-averaged models of the Pentland Firth. Both Refs. [18] and [5] find a value of $c_b = 0.005$ to give a closer match with measured ADCP data, which is higher than the typical value of $c_b = 0.0025$ often used in ocean models. Ref. [16] also seems to favour a higher bottom friction coefficient, although there is some ambiguity in their definition of the bottom friction term. Ref. [5] argue that this higher value may be ascribed to the exposed bedrock found in most of the Pentland Firth.

It was observed that the choice of bottom friction coefficient had little overall impact on the tidal gauge comparison. In Table 3 the RMS errors (in cm) are shown between modelled and harmonically reconstructed measurements at the gauges for two values of the bottom friction coefficient $c_b = 0.0025$ and $c_b = 0.005$. No significant difference in model errors in the free surface prediction was observed at the tidal gauges.

Since the main feature of interest for this study are the currents in the Inner Sound, a comparison with ADCP data located within the turbine array area (see Fig. 1) was used to further validate the model To assess the outcomes of this comparison we used bias in speed and direction, the RMS error in speed, and the scatter index, and the correlation coefficient. See e.g. Ref. [7] for details on how these statistics were calculated.

In Table 4 it can be seen that with a standard value of $c_b = 0.0025$ the currents, during both ebb and flood, are overestimated in the model. The value $c_b = 0.005$ changes this to a smaller underestimation of the current speeds. Also the direction of the tidal current during ebb improves with the higher bottom friction value. A directional bias during the flood remains. This is likely due to the much more complicated flow structure during the flood where the ADCP is located in a boundary current coming off the island of Stroma. Strong gradients in the flow mean that the results will be very sensitive to the exact location of the ADCP within that flow pattern. Data from multiple ADCP locations would be required to investigate potential differences in the spatial variation of the flow field. Based upon the results presented in this section a background friction value of $c_b = 0.005$ was used in all further simulations.

3. Results and discussion

3.1. Model prediction: unimpeded flow

Model predictions of current velocities within the Inner Sound compare well with previously published modelling studies [17] and measurements [26]. As expected, the highest velocities follow the deepest parts of the channel and thus are generally concentrated in a narrow 'core' in the centre of the Inner Sound. During flood the tidal flow enters the Inner Sound from the north-west and is deflected south-east by the southern tip of Stroma. Consequently, a strong velocity gradient forms east of the Stroma Skerries. Flow velocities within the central part of the channel are seen to exceed 3 ms^{-1} for a significant proportion of each flood tide. During ebb flow peak velocities are slightly lower and move north, away from the centre of the channel. Flow enters the Inner Sound from the east, but is deflected north-west by the Stroma Skerries and the core of the flow passes south of the sediment wedges as shown in Ref. [26]. This results in the formation of clockwise moving eddy structures west of Stroma. Fig. 6 shows a map of the Inner Sound displaying the difference between mean current velocities over a full 30 day tidal cycle of the simulation. This figure strongly suggests that the Inner Sound experiences an asymmetric tidal regime with mean velocities in the central and southern parts of the channel being greatest during flood. Note the ebb flow is greatest north of the sediment wedge, whereas the flood flow is south of the

Table 3
RMS error (in cm) in free surface elevation in the period between high and low water at spring and neap tide as a percentage of the range (high water minus low water level). Model output for two different values of the bottom friction coefficient c_b, is compared with free surface elevations reconstructed from harmonic constituents available at six different gauge locations.

	Scrabster		Stromness		Kirkwall		Wick		Station-S5		Station-53	
	Spring	Neap	Spring	Neap	Spring	Neap	Spring	Neap	Spring	Neap	Spring	Neap
$c_b = 0.0025$	2.4	1.5	4.8	4.4	2.3	4.7	1.6	1.6	1.0	0.9	4.4	3.0
$c_b = 0.005$	2.8	1.6	4.2	3.6	3.7	3.7	2.0	1.5	1.0	0.9	4.4	3.2

Table 4
Statistics used to compare modelled tidal currents (using two different bottom friction values) and a reconstruction from harmonic constituents at an ADCP location in the Inner Sound.

	Speed bias ebb (m/s)	Speed bias flood (m/s)	Speed RMS error (m/s)	Speed scatter index	Speed correlation coefficient	Direction bias ebb (deg)	Direction bias flood (deg)
$c_b = 0.0025$	0.26	0.22	0.44	0.18	0.94	13	−24
$c_b = 0.005$	−0.19	−0.15	0.39	0.17	0.97	13	−24

wedge (as shown in Fig. 3). This difference of flow structures is also shown in Ref. [26] (their Fig. 6a). This implies a net movement of sediment from west to east in the southern part of the channel, but a net movement east to west in the northern part. However, ebb tidal velocities are dominant in some regions of the channel, particularly along the north-eastern coast of Stroma, where there is a net flow northwards from both ebb and flood tides to the northwards of Stroma, with particularly high residual currents. Thus, any sediment deposited in regions of low flow during one half of the tidal cycle is likely to be re-mobilised by the next. The placement of a tidal array within the centre of the Inner Sound is likely to deflect flow during both flood and ebb, perhaps exposing some regions to longer term sediment accumulation or removing existing sediment accumulations [17]. In addition, there is a zone of very low (near zero) residual current to the south of Stroma, which aligns with the sediment wedge as shown in Fig. 3).

In order to produce maps of possible sediment accumulation sites within the Pentland Firth, bed shear stress data output by Fluidity were coloured according to typical values of τ_c for coarse sand, fine gravel and medium gravel (Table 1), indicating the regions in which these sediment types might accumulate if they were present in the flow. After each model run, one such sediment accumulation map was produced for peak flood (eastwards flow) and peak ebb (westward flow), thus showing the likely locations of sediment build-up during these tidal stages. A further map was then produced from maximum and mean bed shear stress data over a 30 day tidal cycle, showing the likely locations of long term sediment accumulation. Fig. 7 shows maps of bed shear stress distribution for peak flood and ebb tide in the unimpeded case. These maps are in broad agreement with [17] in that they show the development of an elongated bar region of coarse sand off the Southern tip of Stroma and its subsequent erosion during ebb tide. Our results are also similar to those shown in Refs. [26]; but some details, especially on the ebb tide are different within the main channel south of Stroma. However, this work predicts that any sediment in the southern part of the channel would only collect in Gills Bay and should not extend into deeper parts of the channel as shown by Ref. [17]. This prediction is in closer agreement with the bathymetry and is perhaps a result of the bathymetry used. It is also encouraging to note the predicted regions of low bed shear stress along the south-western edge of the map along the coast and north-west of Swona which are in agreement with the benthic environment map presented in Ref. [45].

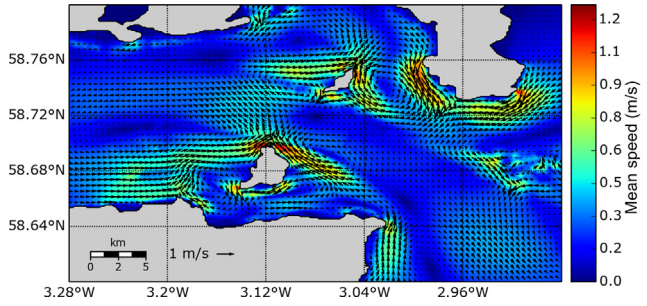

Fig. 6. Mean velocity magnitude over the first 30 days of the simulation with vectors showing the mean tidal current. Residual currents show the position of eddies during the ebb (east-west flow) and flood (west-east flow). The high flow magnitudes show the high asymmetry in the tidal flow in this region.

3.2. Model prediction: increasing array size

Figs. 9 and 8 show the predicted patterns of sedimentation and erosion associated with flood and ebb tide for array sizes of 85 and 400 turbines. These maps reveal much about how the presence of tidal turbines could potentially affect sediment transport in the region. In each case, the turbine array is seen to divert peak flows away from the centre of the Inner Sound and increase bed shear stress close to its boundaries.

During flood this effect becomes highly pronounced (Fig. 8), which indicates that the presence of 400 turbines has the potential to reshape or remove the bar of sediment that forms at the southern tip of Stroma at flood tide. In the case of 400 turbines (Fig. 8), mean values of bed shear stress within the Inner Sound decrease by around 25 Nm^{-2} from their values in the unimpeded case (Fig. 10). This decrease is particularly acute downstream of the

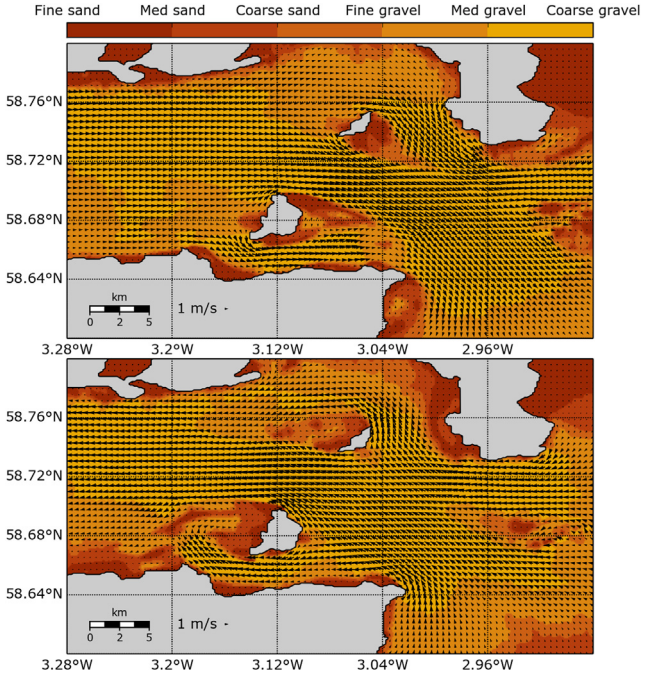

Fig. 7. Simulated sediment accumulation maps for the unimpeded case with flood (west-east flow) top and ebb (east-west flow) bottom. If sediment is present in the flow, these maps show the possible zones in which it might be deposited based on bed shear stress τ. Colours show the *minimum* grain size that could occur there. The significant differences between ebb and flood suggest that any sediment that is deposited is likely to be removed in the next tidal cycle apart from localised regions. Vectors show direction and magnitude of the instantaneous flow. (For interpretation of the references to colour in this figure legend, the reader is referred to the web version of this article.)

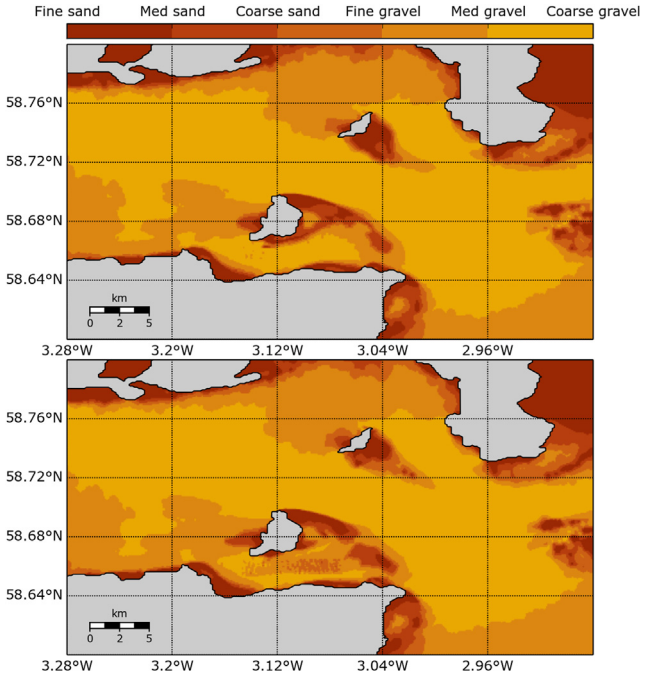

Fig. 8. Simulated sediment accumulation maps for 85 (top) and 400 (bottom) turbines during peak flood (west-east flood). When compared to Fig. 7, the 85 turbine array appears to have a relatively minor impact upon the distribution of flow within the Pentland Firth. In contrast, the 400 turbine array appears to cause more substantial changes, with modifications in the distributions of sediment in the eddy to the east of Stroma. As in the ebb case, the eastern wake of Swona is also modified.

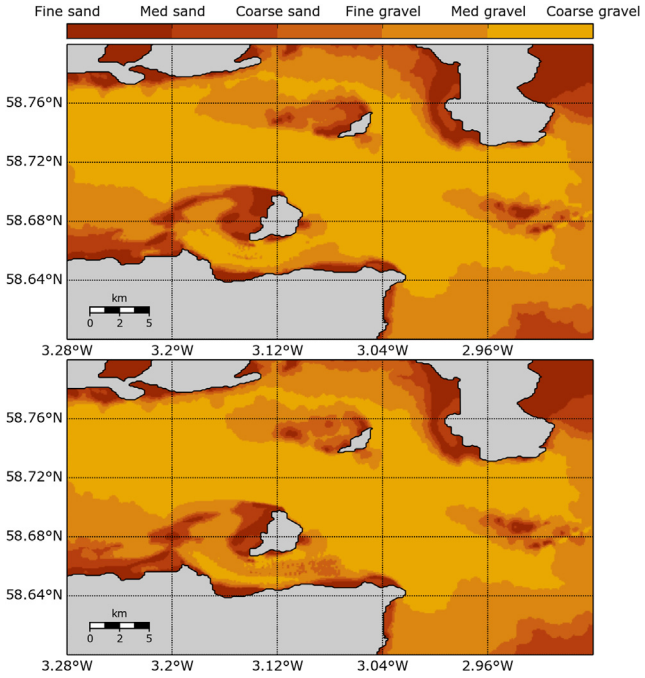

Fig. 9. Estimated sediment maps for 85 (top) and 400 (bottom) turbines during peak ebb (east-west flow). Increasing array size causes peak flows to migrate away from the centre of the Pentland Firth, where a band of coarse sand or fine gravel may develop. The wake around Stroma is substantially affected as expected, with reduced flow (finer grain sizes) in the array wake and into the eddy west of Stroma. Effects of the turbine emplacement are seen around Swona, some 15–20 km array from the array.

turbines and is sufficient to allow for the deposition of large regions of fine gravel and sand, particularly within the array itself. There is also significant erosion along the sides the tidal array due to diversion of the flow around it. Most changes are evident in a region around 15 km in the immediate vicinity of the turbine array. Note the modifications of the wake around Swona are not seen in the mean bed shear stress but are in the maximum bed shear stress.

During flood tide the turbine array is seen to develop a significantly modified wake structure (Figs. 8 and 10). In the cases of 400 turbines, significant velocity shear zones develop north and south of the array as peak flow velocities are diverted towards the boundaries of the Inner Sound. This in turn affects the distribution of sediment accumulation around Stroma. Generally the presence of a tidal array is predicted to increase the volume of sediment within the Inner Sound, although much of this extra sediment is likely to build up in transient features that migrate according to the tides. The difference between the case with turbines and the unimpeded flow (e.g. Fig. 10) indicates relatively minor changes in the positions of regions of long term sediment accumulation below 85 turbines. However, the step from 85 to 240 turbines sees the development of a fine gravel deposit within the array itself, the extent of which grows further in the case of 400 turbines (Fig. 10).

The ebb tide shows similar effects. Fig. 9 indicates that accumulation of fine gravel may begin to occur within the turbine array after its rating exceeds approximately 85 MW during the ebb tide. Such accumulations may not hinder the operation of the turbines, but may increase maintenance costs and also may alter the distribution of benthic organisms within the Inner Sound [45]. A reduction of flow velocities through the Inner Sound also appears to affect the sediment transport regime elsewhere in the Pentland Firth, although it is difficult to determine a general pattern. During ebb tide, the large region of low bed shear stress west of Stroma appears to be modified with increasing numbers of turbines, although its northern limit remains fairly constant due to exceptionally high currents in the Outer Sound. An increase in flow

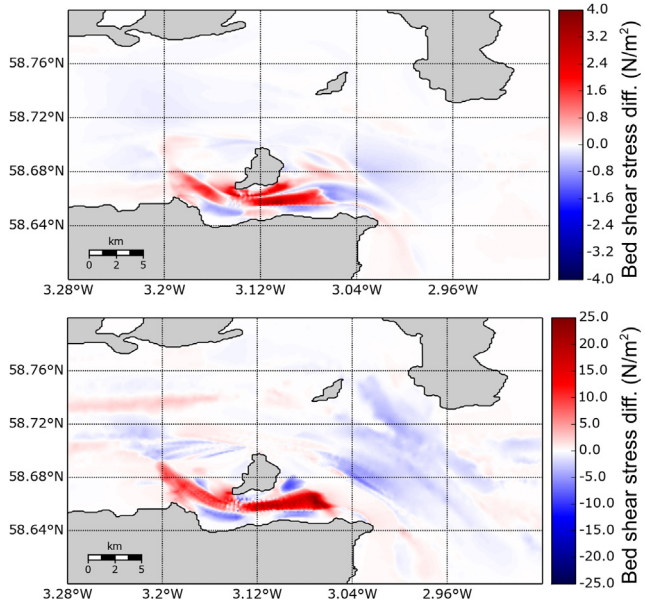

Fig. 10. Map of the Inner Sound showing the difference between the distribution of mean bed shear stress (top) and maximum bed shear stress (bottom) in the case of zero and 400 turbines over the first 30 days of simulation. Positive numbers indicate that the unimpeded case gave *larger* bed shear stress than with 400 turbines; negative numbers means the case with 400 turbines produced larger bed shear stresses. The maximum difference of 4 N/m^2 is equivalent of changes of medium sand to fine gravel and 25 N/m^2 is equivalent of going from medium sand to coarse gravel (see Table 1).

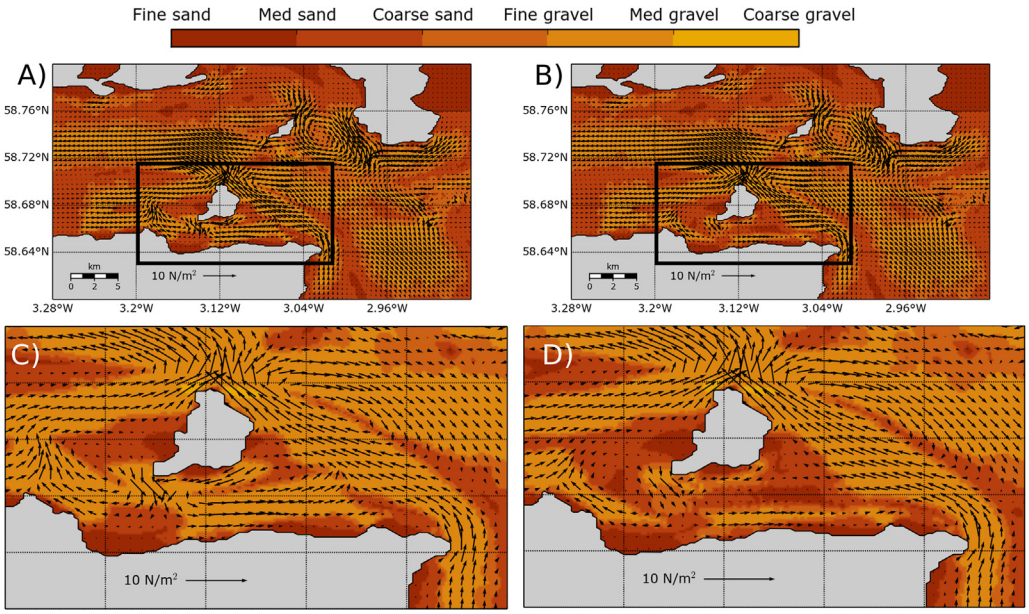

Fig. 11. The effect of adding 400 turbines on the mean bed shear stress direction over the first 30 days of the simulation. A) Unimpeded flow simulation with shading showing approximate minimum grain size and vectors showing the direction and magnitude of the mean bed shear stress. B) Same as A) but with 400 turbines. C) Close-up of the array area from A). D) Close-up of the array area from B). There is modification to the flow vectors to the south of Stroma within the array, in Gills Bay and along the coast to the east of the array. Effects are limited to a region at most 10 km from the array.

velocities as two "jets" to the north and south of the array during ebb tide appears to modify the zone of sediment accumulation west of Stroma. Such zones of sediment accumulation may have their own effects upon flow distribution, perhaps serving to further modify velocities within the Inner Sound over the long term.

The presence of turbines also affects the residual tidal currents (Fig. 11). Effects are largely restricted to an area of around 10 km around the Inner Sound. The presence of 400 turbines reduces the eastward flow in the centre of the channel and this in turn results in deposition within the turbine array. There is a weakening of the residual current to the west of Stroma, resulting in a larger area of potential finer sediment deposition. The effects to the east of Stroma are limited to within a few kilometres of the turbine array.

4. Outlook

This study has highlighted the need to understand the potential changes in sediment pathways due to the emplacement of tidal marine turbine arrays. Our main finding from several simulations is that large deployments have the potential to cause sediment to accumulate within the array whilst altering erosion either side of and around the array. The area over which the effect of a tidal turbine array is seen, of course, varies with the size of the array. Small arrays have negligible effects at the far-field and regional scale. Once the array is of the order of 200 MW, the array produces effects at approaching the far-field scale, as shown in other studies [2,37]. There are, however, limitations to the results presented here.

The lack of information on the suspended sediment load and existing pathways makes modelling sediment pathway changes difficult. Our model agrees well with the sedimentary features that can be seen on two independent bathymetries (Fig. 3 and [17]). However, the literature suggests that these may be transient features – easily reworked by storms. Without more data on the sediment pathways in the area it is difficult to conclude what the long term effects of a tidal turbine array might be.

The representation of the turbines within the model and a depth-averaged approach does not allow for changes in velocity with depth to be assessed. Although using Fluidity's parallel scaling performance it would certainly be feasible to extend the model to multiple layers, it would still come at significant cost. Furthermore significant work would have to go into the validation of the turbulent wake structure behind the turbines to be able to obtain a reliable prediction of the vertical structure of the near field flow. Nevertheless, such a model could provide valuable insights into changes of sediment dynamics in and near the farm area itself and would therefore be very useful for both operational purposes and environmental impact studies.

The results shown here show major near-field and minor far-field changes to sediment pathways due to arrays of above 85 turbines – below the currently proposed maximum array size. Most of the changes occur within close proximity to and within the array site, with substantial potential to accumulate sediments within the array and erosion of any existing surrounding sediment. This may have effects on coastal deposition in the area, but will most likely result in migration of existing sandbanks towards the lee of Stroma. Benthic fauna in the area could also be affected by changes in sediment accumulation, but nearby locations offer similar or identical conditions to those found in the Inner Sound and it is likely that no regional effects on benthic fauna will be seen. Also, the positive habitat-creation potential of marine developments have been discussed in the context of offshore wind [52].

5. Conclusion

A multiscale resolution depth-averaged model, with resolution varying from 18 m to 20 km, has been used to simulate the placement of tidal energy turbines in the Inner Sound. This model can resolve individual turbines as a drag force applied over a number of mesh entities using this multiscale capability. The model has been validated against a number of tidal gauges and ADCP data in the region and provides good agreement to sea surface elevation changes and current velocities. Using this model, it can be shown that the placement of turbines has an effect on the local flow field,

which in turn can have regional effects on the sediment routing in the area.

It is clear that the Inner Sound of Stroma offers a useful tidal resource, which has rightfully attracted significant commercial interest for the placement of tidal arrays. Although this region is generally classified as sediment starved [45], local accumulations of coarse sand and gravel do exist and are predicted to migrate within the Inner Sound according to differences in flow conditions between ebb and flood tide. The Pentland Firth experiences significant tidal asymmetry, meaning that there is a net movement of sediment from west to east under natural conditions. However, the placement of tidal arrays with capacities in excess of 85 MW within the Inner Sound is likely to effect natural patterns of sediment migration. As flow is diverted around the turbines the most favourable region for sediment accumulation moves to the centre of the array, where long term accumulations of gravel and coarse sand may develop. Scouring and removal of existing sediment deposits to the north and south of the array is also expected to occur. These effects are unlikely to affect the operation of the turbines here due to the low sediment levels in the area. Finally, it should be stated that our results are somewhat indicative in that we are using idealised turbines, but nevertheless changes in sediment routing should be considered for other potential turbine sites.

Acknowledgements

The authors would like to thank MeyGen Ltd. for supplying bathymetry and ADCP data, and Sarah Crammond in particular for useful discussions and comments. Comments from two anonymous reviewers helped to substantially improve this paper. This work was supported by the UK's Engineering and Physical Sciences Research Council under grant EP/J010065/1; RM-S was funded by the Royal Geological Society summer student programme. The simulations were carried out on Imperial College London's HPC service, CX2.

References

[1] Adcock TA, Draper S, Houlsby GT, Borthwick AG, Serhadlıoğlu S. The available power from tidal stream turbines in the Pentland Firth. Proc R Soc A: Math Phys Eng Sci 2013;469(2157):20130072.
[2] Ahmadian R, Falconer R, Bockelmann-Evans B. Far-field modelling of the hydro-environmental impact of tidal stream turbines. Renew Energy 2012;38(1):107–16.
[3] Balay S, Brown J, Buschelman K, Eijkhout V, Gropp W, Kaushik D, et al. PETSc users manual revision 3.4. 2013.
[4] Basford D, Eleftheriou A. The benthic environment of the North Sea (56 to 61N). J Mar Biol Assoc U. K 1988;68(01):125–41.
[5] Baston S, Harris R. Modelling the hydrodynamic characteristics of tidal flow in he Pentland Firth. In: Proceedings European Wave and Tidal Energy Conference. No. 317; 2011. p. 7.
[6] Berenbrock C, Tranmer AW. Simulation of flow, sediment transport, and sediment mobility of the lower coeur dalene river, idaho. Tech. Rep. 2008-5093. USGS; 2008.
[7] Brière C, Abadie S, Bretel P, Lang P. Assessment of TELEMAC system performances, a hydrodynamic case study of Anglet, France. Coast Eng 2007;54(4):345–56.
[8] Bryden IG, Couch SJ, Owen A, Melville G. Tidal current resource assessment. Proc Inst Mech Eng Part A J Power Energy Mar. 2007;221:125–35.
[9] Connor D, Gilliland P, Golding N, Robinson P, Todd D, Verling E. Ukseamap: the mapping of the seabed and water column features of UK Seas. Tech. rep. Peterborough: Joint Nature Conservation Committee; 2006.
[10] Cotter CJ, Ham DA. Numerical wave propagation for the triangular P1DG–P2 finite element pair. J Comput Phys 2011;230(8):2806–20.
[11] Cotter CJ, Ham DA, Pain CC. A mixed discontinuous/continuous finite element pair for shallow-water ocean modelling. Ocean Model 2009;26:86–90.
[12] Cotter CJ, Ham DA, Pain CC, Sebastian R. LBB stability of a mixed Galerkin finite element pair for fluid flow simulations. J Comput Phys 2009;228(2):336–48.
[13] Couch SJ, Bryden I. Tidal current energy extraction: hydrodynamic resource characteristics. Proc Inst Mech Eng Part M J Eng Marit Environ Dec. 2006;220:185–94.
[14] Davies AM, Kwong SCM. Tidal energy fluxes and dissipation on the European continental shelf. J Geophys Res Oceans 2000;105:21969–89.
[15] Divett T, Vennell R, Stevens C. Optimisation of multiple turbine arrays in a channel with tidally reversing flow by numerical modelling with adaptive mesh. Philos Trans R Soc A Math Phys Sci 2013.
[16] Draper S, Adcock TAA, Borthwick AGL, Houlsby GT. Estimate of the tidal stream power resource of the Pentland Firth. Renew Energy Mar. 2014;63(0):650–7.
[17] Easton M, Harendza A, Woolf D. Characterisation of a tidal energy site: hydrodynamics and seabed structure. In: 9th European Wave and Tidal Energy Conference. EWTEC; 2011.
[18] Easton MC, Woolf DK, Bowyer PA. The dynamics of an energetic tidal channel, the Pentland Firth, Scotland. Cont Shelf Res Oct. 2012;48:50–60.
[19] Edina Digimap Service. Hydrospatial one, gridded bathymetry. 2014. http://edina.ac.uk/digimap/. downloaded 2014.
[20] Egbert GD, Erofeeva SY. Efficient inverse modeling of barotropic ocean tides. J Atmos Ocean Technol 2002;19(2):183–204.
[21] Farrow GE, Allen NH, Akpan EB. Bioclastic carbonate sedimentation on a high-latitude, tide-dominated shelf; Northeast Orkney Islands, Scotland. J Sediment Res 1984;54(2):373–93.
[22] Ford R, Pain CC, Piggott MD, Goddard AJH, de Oliveira CRE, Umpleby AP. A nonhydrostatic finite-element model for three-dimensional stratified oceanic flows. Part I: model formulation. Mon Weather Rev 2004;132(12):2816–31.
[23] Funke SW, Farrell PE, Piggott MD. Tidal turbine array optimisation using the adjoint approach. Renew Energy 2014;63:658–73.
[24] Garrett C, Cummins P. The efficiency of a turbine in a tidal channel. J fluid Mech 2007;588:243–51.
[25] Geuzaine C, Remacle J-F. Gmsh: a 3-D finite element mesh generator with built-in pre- and post-processing facilities. Int J Numer Methods Eng 2009;79(11):1309–31.
[26] Goddijn-Murphy L, Woolf DK, Easton MC. Current patterns in the inner sound (Pentland Firth) from underway ADCP data. J Atmos Ocean Technol 2013;30(1):96–111.
[27] Hasegawa D, Sheng J, Greenberg DA, Thompson KR. Far-field effects of tidal energy extraction in the Minas Passage on tidal circulation in the Bay of Fundy and Gulf of Maine using a nested-grid coastal circulation model. Ocean Dyn 2011;61(11):1845–68.
[28] Hiester HR, Piggott MD, Allison PA. The impact of mesh adaptivity on the gravity current front speed in a two-dimensional lock-exchange. Ocean Model 2011;38(1–2):1–21.
[29] Hill J, Piggott MD, Ham DA, Popova EE, Srokosz MA. On the performance of a generic length scale turbulence model within an adaptive finite element ocean model. Ocean Model 2012;56:1–15.
[30] Huthnance J. Physical oceanography of the North sea – North sea: environment and sea use planning. Ocean Shorel Manage 1991;16:199–231.
[31] Imperial College London, AMCG, 04 2014. Fluidity manual v4.1.11.
[32] Janeković I, Powell B. Analysis of imposing tidal dynamics to nested numerical models. Cont Shelf Res 2012;34:30–40.
[33] Kuzmin D. A vertex-based hierarchical slope limiter for p-adaptive discontinuous galerkin methods. J Comput Appl Math 2010;233(12):3077–85.
[34] Mitchell AJ, Uličný D, Hampson GJ, Allison PA, Gorman GJ, Piggott MD, et al. Modelling tidal current-induced bed shear stress and palaeocirculation in an epicontinental seaway: the Bohemian Cretaceous Basin, Central Europe. Sedimentology 2010;57(2):359–88.
[35] Myers L, Bahaj A, Retzler C, Ricci P, Dhedin J-F. Inter-device spacing issues within wave and tidal energy converter arrays. In: Third International Conference on Ocean Energy; 2010. p. 6.
[36] National Oceanographic Centre, 2011. Harmonic constituents at several gauge locations. Personal Communication with J. Eric Jones.
[37] Neill SP, Jordan JR, Couch SJ. Impact of tidal energy converter (TEC) arrays on the dynamics of headland sand banks. Renew Energy 2012;37(1):387–97.
[38] Neill SP, Litt EJ, Couch SJ, Davies AG. The impact of tidal stream turbines on large-scale sediment dynamics. Renew Energy 2009;34(12):2803–12.
[39] Pain CC, Piggott MD, Goddard AJH, Fang F, Gorman GJ, Marshall DP, et al. Three-dimensional unstructured mesh ocean modelling. Ocean Model 2005;10(1–2):5–33. the Second International Workshop on Unstructured Mesh Numerical Modelling of Coastal, Shelf and Ocean Flows.
[40] Pain CC, Umpleby AP, de Oliveira CRE, Goddard AJH. Tetrahedral mesh optimisation and adaptivity for steady-state and transient finite element calculations. Comput Methods Appl Mech Eng 2001;190(29–30):3771–96.
[41] Peraire J, Persson P-O. The compact discontinuous Galerkin (CDG) method for elliptic problems. SIAM J Sci Comput 2008;30(4):1806–24.
[42] Piggott MD, Gorman GJ, Pain CC, Allison PA, Candy AS, Martin BT, et al. A new computational framework for multi-scale ocean modelling based on adapting unstructured meshes. Int J Numer Methods Fluids 2008;56(8):1003–15.
[43] Piggott MD, Pain CC, Gorman GJ, Power PW, Goddard AJH. h, r, and hr adaptivity with applications in numerical ocean modelling. Ocean Model 2005;10(1–2):95–113. the Second International Workshop on Unstructured Mesh Numerical Modelling of Coastal, Shelf and Ocean Flows.
[44] Rollings E. MeyGen phase 1 EIA scoping document. 2011.
[45] Shields MA, Dillon LJ, Woolf DK, Ford AT. Strategic priorities for assessing ecological impacts of marine renewable energy devices in the Pentland Firth (Scotland, UK). Mar Policy 2009;33(4):635–42.
[46] Shields MA, Woolf DK, Grist EP, Kerr SA, Jackson A, Harris RE, et al. Marine renewable energy: the ecological implications of altering the hydrodynamics of the marine environment. Ocean Coast Manage 2011;54(1):2–9.

[47] Warren I, Bach H. MIKE 21: a modelling system for estuaries, coastal waters and seas. Environ Softw 1992;7(4):229–40.
[48] Wells MR, Allison P a, Hampson GJ, Piggott MD, Pain CC. Modelling ancient tides: the upper carboniferous epi-continental seaway of Northwest Europe. Sedimentology 2005;52(4):715–35.
[49] Wells MR, Allison PA, Piggott MD, Gorman GJ, Hampson GJ, Pain CC, et al. Numerical modeling of tides in the Late Pennsylvanian Midcontinent seaway of North America with implications for hydrography and sedimentation. J Sediment Res 2007;77(10):843–65.
[50] Wells MR, Allison PA, Piggott MD, Hampson GJ, Pain CC, Gorman GJ. Tidal modeling of an ancient tide-dominated seaway, part 1: model validation and application to global early Cretaceous (Aptian) tides. J Sediment Res 2010;80(5):393–410.
[51] Wessel P, Smith WHF. A global self-consistent, hierarchical, high-resolution shoreline database. J Geophys Res April 1996;101(B4):8741–3.
[52] Wilson JC, Elliott M. The habitat-creation potential of offshore wind farms. Wind Energy 2009;12(2):203–12.
[53] Wu Y, Chaffey J, Greenberg DA, Colbo K, Smith PC. Tidally-induced sediment transport patterns in the upper Bay of Fundy: a numerical study. Cont Shelf Res 2011;31(19–20):2041–53.